Langmuir

Article

pubs.acs.org/Langmuir

Galvanically Replaced Hollow Au−Ag Nanospheres: Study of Their Surface Plasmon Resonance

Yoonjung Choi,[†] Soonchang Hong,[†] Lichun Liu,[†] Seong Kyu Kim,* and Sungho Park*[,†,‡]

[†]Department of Chemistry and [‡]Department of Energy Science, SKKU Advanced Institute of Nanotechnology, Sungkyunkwan University, Suwon 440-746, South Korea

Supporting Information

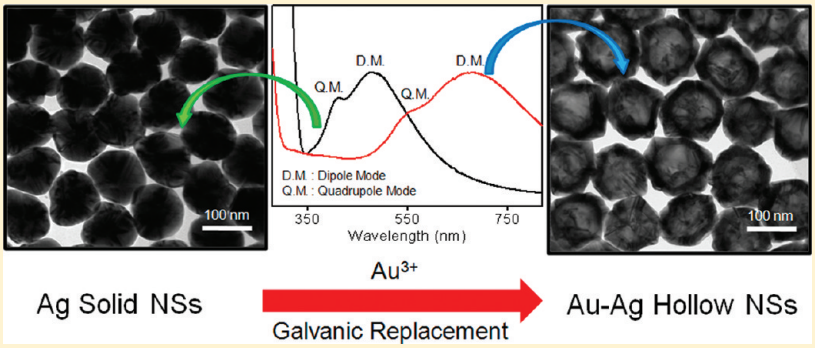

ABSTRACT: We synthesized hollow Au−Ag nanospheres (NSs) by employing a galvanic replacement reaction between $HAuCl_4$ and Ag NSs. Uniform Ag NSs with controllable sizes were synthesized as sacrificial templates by a seed-mediated strategy. The atomic ratio of Au to Ag in Au−Ag NSs was tunable by controlling the reagent concentration. UV−vis extinction spectra acquired from well-dispersed colloidal NS solutions were used to investigate the optical properties of the solutions. In addition to a common dipole mode exhibited on most transition metal nanoparticles, we observed a quadrupole plasmon resonance mode when the diameters of the Ag and Au−Ag NSs were larger than 100 nm. The quadrupole and dipole peaks both shifted to longer wavelengths with increased Au content in Au−Ag NSs. The experimental observation of optical properties of hollow Au−Ag NSs was compared with the theoretical simulation using DDA calculation, showing a good agreement.

1. INTRODUCTION

An alternating electric field of light waves can coherently oscillate with the loosely bound surface electrons on nanoscale metallic structures, resulting in localized surface plasmon resonance (LSPR).[1] LSPR properties have been found to be sensitive to the size, shape, composition, local environment, and dielectric constant of metallic nanoparticles.[2] The dipole mode is most commonly observed in LSPR for colloidal nanoparticles, which is induced by an electric field that moves free electrons resonantly in parallel oscillation away from or back to the metal surface during wave propagation. When the diameters of nanoparticles are close to or less than the wavelength of the incident light, the dipole mode emerges without any other resonance modes. When the sizes of the nanoparticles are sufficiently large, however, higher order plasmonic wave modes such as quadrupole modes have been experimentally observed[3] by UV−vis−NIR spectroscopy, in accordance with the theoretical prediction[4,5] of discrete dipole approximation (DDA). Extensive research on LSPR in metallic nanoparticles has focused on Au and Ag due to their highly active optical properties in visible spectral window. Therefore, a wealth of colloidal solid Ag nanoparticles (spheres,[6] bars,[7] rods,[8] prisms,[9−13] and bipyramids[14−16]), colloidal solid Au nanoparticles (spheres,[17] rods,[18,19] prisms,[19,20] hexagonal plates,[21] concave cubes,[22] trisoctahedral shapes,[23] and tetrahexahedral shapes,[24] nanoshell[25,26]), and their hybrid nanostructures[5,27,28] have been synthesized and characterized based on the optical properties.

The driving force in LSPR research on nanoparticles is the intense interest in fundamental studies and potential applications in sensors, photonics, photocatalysis, and surface-enhanced Raman spectroscopy. One of the most promising practical applications is to detect binding events on a nanoparticle surface by investigating the LSPR peak position change. Since the selective affinity of individual metal surfaces to certain molecules with functional groups can shift the LSPR peak position, the alloyed metal nanoparticles are capable of detecting multiple analytes in one test. In addition, nanoparticles with a hollow interior are lower in density and higher in ratio of surface area to mass. They are more readily suspended in the solution to maintain homogeneity for longer times without precipitation and provide cost-savings because of lower mass consumption.

Received: July 7, 2011
Revised: April 2, 2012
Published: April 2, 2012

   dx.doi.org/10.1021/la202569q | *Langmuir* 2012, 28, 6670−6676

Synthesis of hollow NSs is not as easy as that of solid NSs. In the past decade, hollow nanostructures have been mainly produced through transformations of reactive precursor nanostructures by chemical galvanic replacement[29] and by exploiting the physical Kirkendall effect.[30,31] Xia et al. have demonstrated that hollow Au nanostructures are achievable using relatively smaller silver NSs[32] and nanocubes[33] as sacrificial templates and gold ions as the galvanic replacement reagent. Optical properties of larger hollow Au−Ag NSs synthesized in a controlled manner have been infrequently reported in the literature.[34] In this work, we demonstrate successful synthesis of hollow Au−Ag NSs and the unusual observation of the quadrupole plasmon resonance mode.

2. EXPERIMENTAL PROCEDURES

A. Chemicals. Silver nitrate ($AgNO_3$, 99.9%), hydrogen tetrachloroaurate(III) hydrate ($HAuCl_4{\cdot}nH_2O$), and cetyltrimethylammonium bromide (CTAB, 99.0%) from Acros and Fluka, L(+)-ascorbic acid ($C_6H_8O_6$, 99.5%) from Kanto, sodium hydroxide (NaOH, 98.0%) from Samchun, sodium tetrahydroborate ($NaBH_4$, 98.0%) from Junsei, and 1-octadecanethiol ($C_{18}H_{38}S$, 98.0%) from Aldrich were used in the experiment. All involved reagents were dissolved in distilled water that was prepared by a Milli-Q water purification system.

B. Instrumentation. A JEM-2100F was used to acquire transmission electron microscopy (TEM) images. Scanning electron microscopy (SEM) images and energy dispersive X-ray spectroscopy (EDS) analyses were obtained using a JEOL 7000F and a JEOL 7600F. UV−vis absorption spectra were taken using an S-3100 spectrophotometer (Scinco).

C. Synthesis of Ag NSs. Ag seeds were prepared by reducing $AgNO_3$ using $NaBH_4$. In detail, 600 μL of 10 mM $NaBH_4$ was cooled at 4 °C in a refrigerator for 15 min and was mixed with 2 mL of 0.25 mM $AgNO_3$ and 18 mL of 0.1 M CTAB in a 20 mL glass vial. After 2 min of stirring, the mixed solution was held at room temperature for ∼2 h until the colorless initial solution turned light yellow. Ag NSs were prepared by mixing 200 mL of 0.1 M CTAB, 5 mL of 0.01 M aqueous $AgNO_3$, 10 mL of 0.1 M aqueous ascorbic acid, 2 mL of 0.1 M aqueous NaOH solution, and the desired amount of Ag seed solution, followed by reacting for ∼4 h at room temperature without stirring. The sizes of Ag NSs were controlled by varying the volume of Ag seed solution. Specifically, 1 mL, 0.1 mL, 40 μL, and 20 μL of Ag seed solutions were used to grow Ag NSs at 30, 60, 80, and 100 nm, respectively. The products were collected by centrifugation at 6000 rpm for 25 min, 5000 rpm for 20 min, 4000 rpm for 20 min, and 4000 rpm for 20 min corresponding to the above solutions. After centrifugation, the top solution was replaced with distilled water. Then, the 10 mL solution was transferred into a Teflon cell, and ∼5 mL of hexane was added to the solution to form a hexane/water interface. Next, 1 mL of 9.17×10^{-8} M 1-octadecanethiol was added dropwise to the top hexane layer, and ∼10 mL of ethanol was added dropwise at a rate of 30 mL/h using a mechanical syringe pump (KDS101). Ethanol was used to extract NSs from the aqueous solution into the hexane/water interface region. The resulting NS film was collected on silicon wafers, and the NSs on copper grids were used for SEM, TEM, and EDS measurements.

D. Galvanic Replacement Reactions. A $HAuCl_4$ solution was prepared by adding 100 μL of a 20 mM aqueous $HAuCl_4$ solution to 10 mL of a 0.05 M CTAB solution. Using the Ag NSs and $HAuCl_4$ solutions, we synthesized the hollow nanostructures using the galvanic replacement reaction for about 12 h at room temperature. The Ag NS solution (20 mL) was mixed with 4, 7, 10, and 30 mL of $HAuCl_4$ solution to generate the hollow nanostructures. Other post-treatment procedures were similar to those described in section C. The concentration of Ag NPs and the required amount of $HAuCl_4$ solution were decided by following procedure. The volume of Ag^+ (5 mL) multiplied by the concentration of Ag^+ (0.01 M) is the number of moles of Ag^+, which is 5×10^{-5} mol. An Ag NS with diameter of 1.4 nm requires ∼100 atoms. Therefore, an Ag NS with diameter of 80 nm has about 2.0×10^7 atoms. So, the concentration of Ag NS is 1.1×10^{-11} M. Experimentally, for the case of Ag NSs with diameter of 80 nm, we added Au(III) species corresponding to one-fifth of total required amount of Au atoms in order to form hollow Au−Ag NS with a shell thickness of ca. 20 nm. When added more than this amount, we observed the shape-collapse of Au−Ag NPs.

E. Discrete Dipole Approximation (DDA) Calculations. The source code for the DDA calculation was obtained from Professor Draine's homepage.[35] Optical constants for Au and Ag were obtained from ref 36. The refractive index dispersion of water was also used.[37] A spherical target with or without a hole is subdivided with an array of cubic cells of 3 nm in size. Interaction between polarizable point dipoles in the cells and incident light wave is solved iteratively, from which the cross sections for extinction and scattering can be generated.

3. RESULTS AND DISCUSSION

Ag NSs were obtained using a seed-mediated synthetic method, producing a broad size range of structures from 20 nm to up to 100 nm and a narrow size distribution of individual samples. The difference in reduction potential between Ag^+/Ag (0.80 V vs SHE) and $AuCl_4^-/Au$ (0.99 V vs SHE)[34] allows $AuCl_4^-$ ions to oxidize Ag atoms in the solution phase, as shown in eq 1. The target Ag NSs were synthesized by growing pregrown Ag seeds to larger desired sizes. Using as-prepared Ag NSs as sacrificial templates, the hollow Au−Ag NSs were then prepared by carrying out a galvanic replacement reaction between Ag NSs and a $HAuCl_4$ solution, as illustrated in Scheme 1.

Scheme 1. Schematic Illustration of Synthesis Procedure

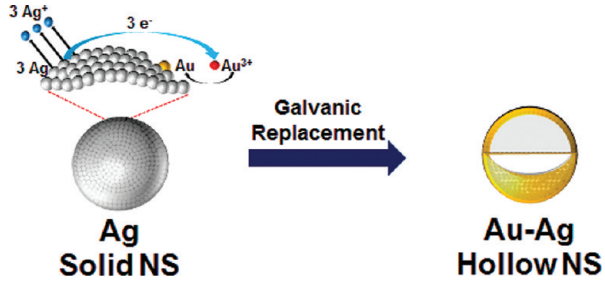

$$3Ag(s) + AuCl_4^- \rightarrow Au(s) + 3Ag^+(aq) + 4Cl^-(aq) \quad (1)$$

During galvanic replacement, it was demonstrated that Au atomic shell was initially deposited on the surface of Ag NSs, which functioned as electron supplier for reduction reaction. Further reduced Au atoms dwelled on the initial Au layer and grew epitaxially, while the core Ag atoms were oxidized and dissolved in the solution. Therefore, the space occupied by Ag atoms unable to be filled by Au atoms resulted in the formation of hollow interior. Ag^+ ions produced by $HAuCl_4$ oxidation diffused out from the Ag NSs more quickly than Au atoms diffused in, resulting in hollow structures.[34−39] This process is similar to that of the Kirkendall void formation.[30] Incomplete replacement may create bimetallic Au−Ag NSs, in which penetrated Au atoms crystallize into face-centered-cubic Ag lattices due to the considerably similar lattice parameters of the two elements (Au, 4.0786 Å; Ag, 4.0862 Å).[35] The atomic ratio of Au to Ag in the final hollow NSs could be rationally tuned by controlling the concentration of the $HAuCl_4$ solution and the reaction time used in the galvanic replacement reaction (see Supporting Information, Figure S1). We found that the hollow

dx.doi.org/10.1021/la202569q | Langmuir 2012, 28, 6670−6676

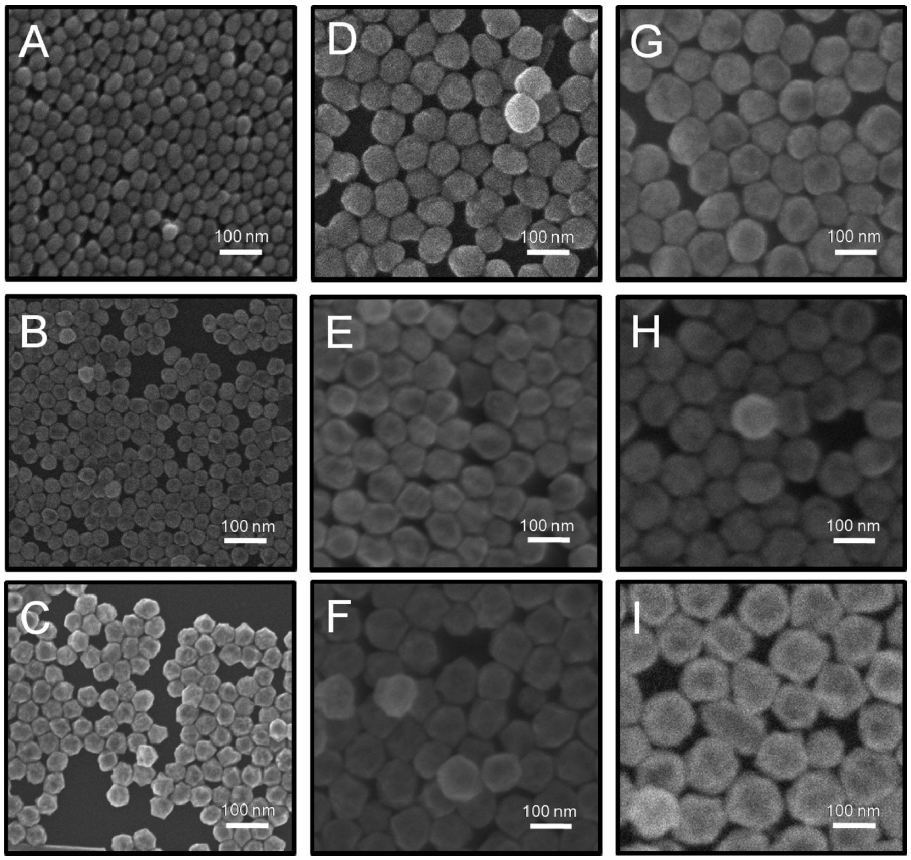

Figure 1. SEM images show the morphology and size of Ag and Au−Ag NSs. (A), (D), and (G) indicate the sizes of Ag NSs, 40 (±3), 83 (±4), and 101 (±7) nm, respectively. By controlling the concentration of $HAuCl_4$ solution used in the Galvanic replacement reaction, we show SEM images (B), (E), (H) at 33.3 μM and 119 μM for (C), (F), (I), corresponding to (A), (D), (G). The sizes of nanoparticles were (B) 45 (±3), (C) 50 (±3), (E) 86 (±4), (F) 97 (±5), (H) 108 (±7), and (I) 128 (±10) nm.

NSs were larger than the original Ag NSs, and they increased with increasing concentration of $HAuCl_4$ solution. Experimental observation revealed that, when a 33.3 μM $HAuCl_4$ concentration was used in the replacement reaction, the average sizes of the resulting NSs increased. The SEM images of each sample are displayed in Figure 1. Furthermore, the surfaces of NSs after the replacement reaction were rougher compared to those of the original Ag NSs due to increased deposition of Au atoms at high-energy sites. The size changes in NSs before and after the replacement reaction were ascribed to the formation of a hollow interior and Au epitaxial growth on Ag NS surface during the replacement reaction.

The hollow interiors of Au−Ag NSs were visible in the high-resolution TEM images of Figure 2B. Their counterparts, solid Ag NSs, are presented in Figure 2A. We employed EDS line analysis to demonstrate the coexistence of Au and Ag in the product. The EDS line analysis in Figure 2C,D reveals the compositions of Ag and Au−Ag NSs. The inset TEM images in (C) and (D) show a single NS to illustrate the clear difference in the interiors of the two samples. As shown, Ag NSs had a solid interior in Figure 2A and the Au−Ag NSs had a hollow interior in Figure 2B. The homogeneity of Ag and Au atom distribution over hollow Au−Ag NSs was confirmed by the large area TEM EDS mapping images, as displayed in Figure 3.

The adopted synthetic method allows easy dispersion of NSs into the liquid phase. We acquired UV−vis extinction spectra of Ag and Au−Ag NSs in distilled water, as shown in Figure 4. The leftmost spectra in (A), (B), and (C) correspond to the different sizes of Ag NSs: (A) 40, (B) 83, and (C) 101 nm, respectively. As the Ag NSs increased in size, the dipole peaks shifted from 442.1 nm for (A), to 453.1 nm for (B), and to 477.8 nm for (C). The obvious red-shift of dipole peaks for Ag NSs agreed well with the known rule that the dipole peak position of NSs varies with size in the same ambient environment.[6,40] Figure 4A shows UV−vis spectra of NSs synthesized with an increased concentration of Au(III) species (indicated by arrow direction), the same situation as in Figure 4B,C. The change in optical properties of each NS sample was visibly indicated by clear color changes, as shown by photographic images in the right upper insets in each panel of Figure 4. The common characteristic of these three cases was that the dipole mode peaks shifted to longer wavelength with increasing Au atomic ratio. Two factors correlated to the peak shift: compositional change and increase in NS size. Dipole peaks of pure Ag and pure Au NSs were around 400 and 520 nm, and an elevated level of Au atoms in Au−Ag NSs induced a red-shift in the dipole peaks. For identical compositions of NSs, the larger the size was, the greater the red-shift was. Thus, the aforementioned size change in Ag NSs induces the dipole peak change. In addition, the larger size and increased roughness of NSs caused peak broadening.

Among the three sets of experiments, a special distinction was observed for larger Ag NSs and their derived Au−Ag NSs; that is, a small peak appeared at a wavelength slightly lower than that of the dipole peak, as shown in Figure 4C. This peak is a quadrupole plasmon resonance mode. With solid Ag NSs,

dx.doi.org/10.1021/la202569q | *Langmuir* 2012, 28, 6670−6676

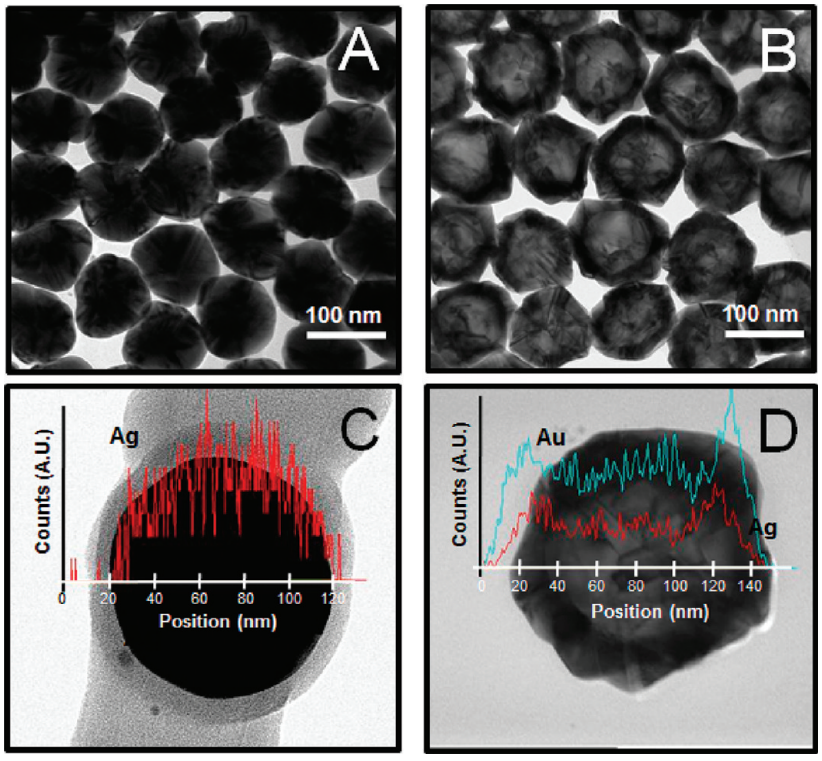

Figure 2. TEM images show solid Ag (A) and hollow Au−Ag (B) and their corresponding EDS line analysis (C) and (D). *Y*-axis indicates peak intensity in arbitrary unit.

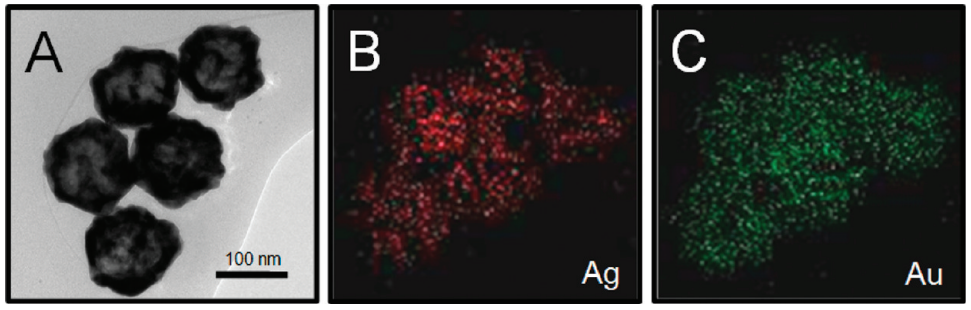

Figure 3. TEM EDS mapping images. (A) TEM image, (B) Ag element distribution, and (C) Au element distribution to the corresponding TEM image sample.

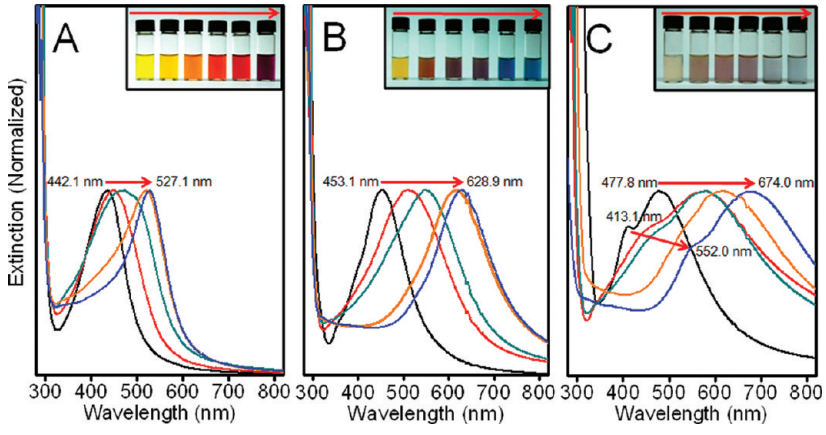

Figure 4. UV−vis spectra show the peak shifting of NSs with increasing the concentration of $HAuCl_4$ solution. (A), (B), and (C) correspond to different sizes of Ag nanoparticles shown in (A), (D), and (G) of Figure 1, respectively. Right upper insets show the color change of resulting NSs solutions when adjusting the concentration of $HAuCl_4$ solution. The arrows were used to denote the direction of increasing concentration of $HAuCl_4$ solution. *Y*-axis indicates peak intensity in arbitrary unit.

dx.doi.org/10.1021/la202569q | *Langmuir* 2012, 28, 6670−6676

the quadrupole was previously reported by the Chumanov group.[41] However, observation of this peak after replacement with Au(III) species is unexpected because of the relatively weak optical activity of Au. In the current system, quadrupole mode peaks are located at a shoulder position on the dipole peaks during the replacement process and were clearly distinguishable in each extinction spectrum. With increasing the size of NS and converting to hollow Au–Ag NSs, the quadrupole peaks shifted to longer wavelengths, as did the dipole peaks. However, the magnitude of the quadrupole peak shift ($\Delta\lambda \approx 140$ nm) was less than that of the dipole peak shift ($\Delta\lambda \approx 195$ nm). Considering that a quadrupole peak was observed on single metal Ag NSs at 100 nm size and a quadrupole peak was not observed on Au NSs of the same size,[42−46] we concluded that the quadrupole peak originated from the formation of hollow NS and the trace amount of Ag component in hollow Au–Ag NSs. In order to observe a higher order surface plasmon resonance band, the phase retardation of oscillating surface electrons needs to be established. The Ag component in Au matrix and the free electrons on the hollow shell may induce effectively such retardation in hollow Au–Ag NSs. The red-shift in the dipole peak for Au–Ag NSs was a result of a synergistic effect of Au compositional increase, size expansion of NSs, and the formation of hollow architecture. The quadrupole peak could be maintained even when Au was the dominant component.

In order to confirm the experimental observation, we carried out theoretical calculations by using a discrete dipole approximation (DDA) method. We calculated an extinction spectrum for each of the following NSs; that is, pure solid Ag NS (d = 101 nm), pure solid Ag NS (d = 128 nm), pure hollow Au NS (outer d = 128 nm and inner d = 88 nm), and alloy hollow $Au_{0.75}$–$Ag_{0.25}$ sphere (outer d = 128 nm and inner d = 88 nm). The outer and inner diameters were measured from TEM images obtained from the sample shown Figure 2B, and the measured values were used for the calculations. Figure 5 represents the calculated spectra. In the experiment, the dipole and the quadrupole modes for pure solid Ag NS (d = 101 nm) were observed at 477.8 and 413.1 nm, respectively. The calculated spectrum (black trace in Figure 5) for the analogous Ag NS exhibited a dipole mode at ca. 480 and a quadrupole mode at ca. 400 nm, showing the good agreement between the experiment and theoretically simulated results. When the size of pure solid Ag NS was increased to 128 nm, the dipole and the quadrupole modes were calculated to red-shift to ca. 560 and 415 nm, respectively (orange trace). However, when the pure solid Ag NS is converted to the pure hollow Au NS, both the dipole and quadrupole modes red-shifted to longer wavelength; the dipole mode shifted to ca. 657 nm and the quadrupole mode to 556 nm (red trace). Whereas, when it was converted to the alloy hollow $Au_{0.75}$–$Ag_{0.25}$ NS, the peak of dipole mode shifted to ca. 645 nm and the quadrupole mode to ca. 552 nm (blue trace). The EDS analysis revealed that the resulting synthesized NSs (d = 128 (±10) nm) are composed of Au (75%) and Ag (25%). However, the calculated spectrum showed the better agreement with the pure hollow Au NS rather than with the alloy hollow $Au_{0.75}$–$Ag_{0.25}$ NS. In general, although there is a slight mismatch in the peak positions, it is obvious that the conversion into hollow nanoparticle leads to the higher degree of red-shifts of the dipole and quadrupole modes, which is in good agreement with the experimental observation.

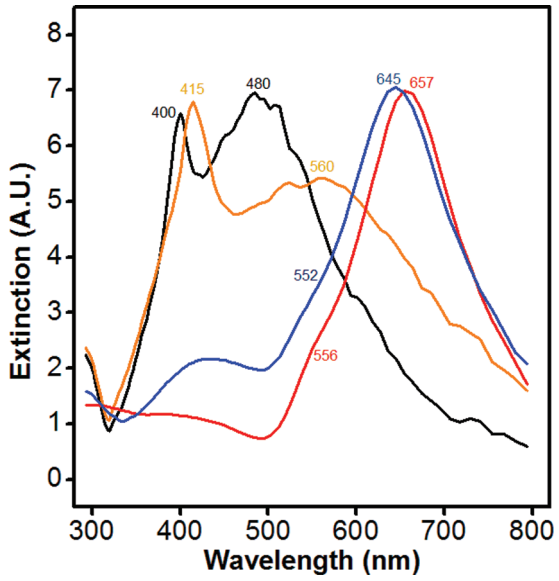

Figure 5. Simulated extinction spectra for pure solid Ag NS (d = 101 nm, black line), pure solid Ag NS (d = 128 nm, orange line), pure hollow Au NS (outer d = 128 nm and inner d = 88 nm, red line), and alloy hollow $Au_{0.75}$–$Ag_{0.25}$ sphere (outer d = 128 nm and inner d = 88 nm, blue line).

4. CONCLUSIONS

In this work, uniform hollow Au–Ag NSs with various sizes were synthesized by adopting a galvanic replacement reaction between $HAuCl_4$ and Ag NSs. Atomic ratios of Au and Ag in Au–Ag hollow NSs were manipulated by controlling the concentration of $HAuCl_4$. Optical characterization revealed that a quadrupole peak also emerged on both larger solid Ag NSs (>100 nm) and synthesized hollow Au–Ag NSs, apart from the dipole peak. Both dipole and quadrupole peaks of NSs red-shifted when their sizes increased and the hollow shell was formed. A quadrupole peak was maintained even when Au was dominant in the hollow Au–Ag NSs.

■ ASSOCIATED CONTENT

Ⓢ Supporting Information

Figures S1–S5. This material is available free of charge via the Internet at http://pubs.acs.org.

■ AUTHOR INFORMATION

Corresponding Author

*E-mail skkim@skku.edu (S.K.K.), spark72@skku.edu (S.P.); Fax 82-31-290-7075.

Notes

The authors declare no competing financial interest.

■ ACKNOWLEDGMENTS

This work was supported by the National Research Foundation of Korea (2011-0027911, 2011-0003385, World Class University (WCU): R31-2008-10029, and Priority Research Centers Program: NRF-20100029699). We also thank Chemical and Biological Detection Research Center Program.

REFERENCES

(1) Lu, X.; Rycenga, M.; Skrabalak, S. E.; Wiley, B.; Xia, Y. Chemical Synthesis of Novel Plasmonic Nanoparticles. *Annu. Rev. Phys. Chem.* **2009**, *60* (1), 167−192.

(2) Kelly, K. L.; Coronado, E.; Zhao, L. L.; Schatz, G. C. The Optical Properties of Metal Nanoparticles: The Influence of Size, Shape, and Dielectric Environment. *J. Phys. Chem. B* **2002**, *107* (3), 668−677.

(3) Kumbhar, A. S.; Kinnan, M. K.; Chumanov, G. Multipole Plasmon Resonances of Submicron Silver Particles. *J. Am. Chem. Soc.* **2005**, *127* (36), 12444−12445.

(4) Zhou, F.; Li, Z.-Y.; Liu, Y.; Xia, Y. Quantitative Analysis of Dipole and Quadrupole Excitation in the Surface Plasmon Resonance of Metal Nanoparticles. *J. Phys. Chem. C* **2008**, *112* (51), 20233−20240.

(5) Kim, S.; Shuford, K. L.; Bok, H.-M.; Kim, S. K.; Park, S. Intraparticle Surface Plasmon Coupling in Quasi-One-Dimensional Nanostructures. *Nano Lett.* **2008**, *8* (3), 800−804.

(6) Stamplecoskie, K. G.; Scaiano, J. C. Light Emitting Diode Irradiation Can Control the Morphology and Optical Properties of Silver Nanoparticles. *J. Am. Chem. Soc.* **2010**, *132* (6), 1825−1827.

(7) Wiley, B. J.; Chen, Y.; McLellan, J. M.; Xiong, Y.; Li, Z.-Y.; Ginger, D.; Xia, Y. Synthesis and Optical Properties of Silver Nanobars and Nanorice. *Nano Lett.* **2007**, *7* (4), 1032−1036.

(8) Pietrobon, B.; McEachran, M.; Kitaev, V. Synthesis of Size-Controlled Faceted Pentagonal Silver Nanorods with Tunable Plasmonic Properties and Self-Assembly of These Nanorods. *ACS Nano* **2008**, *3* (1), 21−26.

(9) Jin, R. Photoinduced Conversion of Silver Nanospheres to Nanoprisms. *Science* **2001**, *294* (5548), 1901−1903.

(10) Xue, C.; Mirkin, C. A. pH-Switchable Silver Nanoprism Growth Pathways. *Angew. Chem.* **2007**, *119* (12), 2082−2084.

(11) Métraux, G. S.; Mirkin, C. A. Rapid Thermal Synthesis of Silver Nanoprisms with Chemically Tailorable Thickness. *Adv. Mater.* **2005**, *17* (4), 412−415.

(12) Zhang, Q.; Hu, Y.; Guo, S.; Goebl, J.; Yin, Y. Seeded Growth of Uniform Ag Nanoplates with High Aspect Ratio and Widely Tunable Surface Plasmon Bands. *Nano Lett.* **2010**, *10* (12), 5037−5042.

(13) Zeng, J.; Xia, X.; Rycenga, M.; Henneghan, P.; Li, Q.; Xia, Y. Successive Deposition of Silver on Silver Nanoplates: Lateral versus Vertical Growth. *Angew. Chem., Int. Ed.* **2011**, *50* (1), 244−249.

(14) Zhang, Q.; Li, W.; Moran, C.; Zeng, J.; Chen, J.; Wen, L.-P.; Xia, Y. Seed-Mediated Synthesis of Ag Nanocubes with Controllable Edge Lengths in the Range of 30−200 nm and Comparison of Their Optical Properties. *J. Am. Chem. Soc.* **2010**, *132* (32), 11372−11378.

(15) Wiley, B. J.; Xiong, Y.; Li, Z.-Y.; Yin, Y.; Xia, Y. Right Bipyramids of Silver: A New Shape Derived from Single Twinned Seeds. *Nano Lett.* **2006**, *6* (4), 765−768.

(16) Zhang, J.; Li, S.; Wu, J.; Schatz, G. C.; Mirkin, C. A. Plasmon-Mediated Synthesis of Silver Triangular Bipyramids. *Angew. Chem., Int. Ed.* **2009**, *48* (42), 7787−7791.

(17) Bonet, F.; Delmas, V.; Grugeon, S.; Herrera Urbina, R.; Silvert, P. Y.; Tekaia-Elhsissen, K. Synthesis of monodisperse Au, Pt, Pd, Ru and Ir nanoparticles in ethylene glycol. *Nanostruct. Mater.* **1999**, *11* (8), 1277−1284.

(18) Smith, D. K.; Miller, N. R.; Korgel, B. A. Iodide in CTAB Prevents Gold Nanorod Formation. *Langmuir* **2009**, *25* (16), 9518−9524.

(19) Millstone, J. E.; Wei, W.; Jones, M. R.; Yoo, H.; Mirkin, C. A. Iodide Ions Control Seed-Mediated Growth of Anisotropic Gold Nanoparticles. *Nano Lett.* **2008**, *8* (8), 2526−2529.

(20) Millstone, J. E.; Park, S.; Shuford, K. L.; Qin, L.; Schatz, G. C.; Mirkin, C. A. Observation of a Quadrupole Plasmon Mode for a Colloidal Solution of Gold Nanoprisms. *J. Am. Chem. Soc.* **2005**, *127* (15), 5312−5313.

(21) Hong, S.; Shuford, K. L.; Park, S. Shape Transformation of Gold Nanoplates and their Surface Plasmon Characterization: Triangular to Hexagonal Nanoplates. *Chem. Mater.* **2011**, *23* (8), 2011−2013.

(22) Zhang, J.; Langille, M. R.; Personick, M. L.; Zhang, K.; Li, S.; Mirkin, C. A. Concave Cubic Gold Nanocrystals with High-Index Facets. *J. Am. Chem. Soc.* **2010**, *132* (40), 14012−14014.

(23) Ma, Y.; Kuang, Q.; Jiang, Z.; Xie, Z.; Huang, R.; Zheng, L. Synthesis of Trisoctahedral Gold Nanocrystals with Exposed High-Index Facets by a Facile Chemical Method. *Angew. Chem., Int. Ed.* **2008**, *47* (46), 8901−8904.

(24) Ming, T.; Feng, W.; Tang, Q.; Wang, F.; Sun, L.; Wang, J.; Yan, C. Growth of Tetrahexahedral Gold Nanocrystals with High-Index Facets. *J. Am. Chem. Soc.* **2009**, *131* (45), 16350−16351.

(25) Wang, H.; Goodrich, G. P.; Tam, F.; Oubre, C.; Nordlander, P.; Halas, N. J. Controlled Texturing Modifies the Surface Topography and Plasmonic Properties of Au Nanoshells. *J. Phys. Chem. B* **2005**, *109* (22), 11083−11087.

(26) Bardhan, R.; Mukherjee, S.; Mirin, N. A.; Levit, S. D.; Nordlander, P.; Halas, N. J. Nanosphere-in-a-Nanoshell: A Simple Nanomatryushka. *J. Phys. Chem. C* **2009**, *114* (16), 7378−7383.

(27) Seo, D.; Yoo, C. I.; Jung, J.; Song, H. Ag−Au−Ag Heterometallic Nanorods Formed through Directed Anisotropic Growth. *J. Am. Chem. Soc.* **2008**, *130* (10), 2940−2941.

(28) Kim, S.; Kim, S. K.; Park, S. Bimetallic Gold−Silver Nanorods Produce Multiple Surface Plasmon Bands. *J. Am. Chem. Soc.* **2009**, *131* (24), 8380−8381.

(29) Lu, X.; Chen, J.; Skrabalak, S. E.; Xia, Y. Galvanic replacement reaction: A simple and powerful route to hollow and porous metal nanostructures. *Proc. Inst. Mech. Eng. N: J. Nanoeng. Nanosyst.* **2007**, *221* (1), 1−16.

(30) Yin, Y. Formation of Hollow Nanocrystals Through the Nanoscale Kirkendall Effect. *Science* **2004**, *304* (5671), 711−714.

(31) Fan, H. J.; Gösele, U.; Zacharias, M. Formation of Nanotubes and Hollow Nanoparticles Based on Kirkendall and Diffusion Processes: A Review. *Small* **2007**, *3* (10), 1660−1671.

(32) Kim, M. H.; Lu, X.; Wiley, B.; Lee, E. P.; Xia, Y. Morphological Evolution of Single-Crystal Ag Nanospheres during the Galvanic Replacement Reaction with HAuCl4. *J. Phys. Chem. C* **2008**, *112* (21), 7872−7876.

(33) Chen, J.; Wiley, B.; McLellan, J.; Xiong, Y.; Li, Z.-Y.; Xia, Y. Optical Properties of Pd−Ag and Pt−Ag Nanoboxes Synthesized via Galvanic Replacement Reactions. *Nano Lett.* **2005**, *5* (10), 2058−2062.

(34) Sun, Y.; Xia, Y. Mechanistic Study on the Replacement Reaction between Silver Nanostructures and Chloroauric Acid in Aqueous Medium. *J. Am. Chem. Soc.* **2004**, *126* (12), 3892−3901.

(35) DDSCAT 7.0, available from http://www.astro.princeton.edu/~draine/DDSCAT.html.

(36) Johnson, P. B.; Christy, R. W. Optical Constants of the Noble Metal. *Phys. Rev. B* **1972**, *6*, 4370−4379.

(37) Daimon, M.; Masumura, A. Measurement of the refractive index of distilled water from the near-infrared region to the ultraviolet region. *Appl. Opt.* **2007**, *46*, 3811−3820.

(38) Sun, Y.; Xia, Y. Alloying and Dealloying Processes Involved in the Preparation of Metal Nanoshells through a Galvanic Replacement Reaction. *Nano Lett.* **2003**, *3* (11), 1569−1572.

(39) Chen, J.; McLellan, J. M.; Siekkinen, A.; Xiong, Y.; Li, Z.-Y.; Xia, Y. Facile Synthesis of Gold−Silver Nanocages with Controllable Pores on the Surface. *J. Am. Chem. Soc.* **2006**, *128* (46), 14776−14777.

(40) Sun, Y.; Mayers, B.; Xia, Y. Metal Nanostructures with Hollow Interiors. *Adv. Mater.* **2003**, *15* (7−8), 641−646.

(41) Khalavka, Y.; Becker, J.; Sönnichsen, C. Synthesis of Rod-Shaped Gold Nanorattles with Improved Plasmon Sensitivity and Catalytic Activity. *J. Am. Chem. Soc.* **2009**, *131* (5), 1871−1875.

(42) Métraux, G. S.; Cao, Y. C.; Jin, R.; Mirkin, C. A. Triangular Nanoframes Made of Gold and Silver. *Nano Lett.* **2003**, *3* (4), 519−522.

(43) Evanoff, D. D.; Chumanov, G. Size-Controlled Synthesis of Nanoparticles. 1. "Silver-Only" Aqueous Suspensions via Hydrogen Reduction. *J. Phys. Chem. B* **2004**, *108* (37), 13948−13956.

(44) Malynych, S.; Chumanov, G. Extinction spectra of quasi-spherical silver sub-micron particles. *J. Quant. Spectrosc. Radiat. Transfer* **2007**, *106* (1−3), 297−303.

(45) Bastús, N. G.; Comenge, J.; Puntes, V. c. Kinetically Controlled Seeded Growth Synthesis of Citrate-Stabilized Gold Nanoparticles of

up to 200 nm: Size Focusing versus Ostwald Ripening. *Langmuir* **2011**, *27*, 11098−11105.
(46) Rodríguez-Fernández, J.; Pérez-Juste, J.; García de Abajo, F. J.; Liz-Marzán, L. M. Seeded Growth of Submicron Au Colloids with Quadrupole Plasmon Resonance Modes. *Langmuir* **2006**, *22* (16), 7007−7010.